CHAPTER 3

THE ROLES OF TEXTURAL FEATURES IN IMPROVING LAND USE AND LAND COVER CLASSIFICATION ACCURACY

3.1 INTRODUCTION

There is increasing attention that the geospatial distribution of LULC is of critical significance in support of sustainable land use planning, natural resource management and environmental monitoring (Lesiv et al., 2016). At present, space-borne remote sensing has been proved as a powerful tool to monitor the Earth's surface, particularly in deriving LULC information and its distribution (Green et al., 1994; Zhu and Woodcock, 2014; Mishra and Rai, 2016).

Nevertheless, LULC classification and information extraction from remote sensing images still remains a challenging task in heterogeneous areas because of several reasons. It is a comprehensive process that involves careful deliberation of different aspects (Lu and Weng, 2007). Other limitations for accurate LULC mapping are the lack of aerial photography, previous LULC maps, and ancillary data (e.g., digital elevation models, geological maps, etc.) that may be helpful in improving the results (Paneque-Gálvez et al., 2013). The presence of spectral confusion caused by land surface features also hampers the training and validation stages during classification process which makes it hard to acquire the classification results with high accuracy. In the last few decades, several classification algorithms including statistics based, non-statistics based, pixel-based to subpixel-based and object-oriented classifiers, have been explored for classifying the multi-source remote sensing images (Lu and Weng, 2007; Szuster et al., 2011; Kumar et al., 2015).

Besides the advancement of classification algorithms, another current research topic is the fair selection of suitable input variables, which may have the same importance as the selection of classifier (Heinl et al., 2009). The remotely sensed data acquired from multiple sensors may have the various potential for LULC classification and mapping. Optical sensor data exhibits spectral, spatial, radiometric, and temporal attributes whereas; radar data have unique features in terms of polarizations (HH, HV, VV, and VH). The radiometric and temporal characteristics of any sensor data are constant. But the spectral and spatial characteristics are the most significant features and need to be further investigated. In case of multispectral datasets, a variety of new variables such as vegetation indices and image transforms can be produced using image processing techniques (Bannari et al., 1995; McDonald et al., 1998). Spectral characteristics of land surface features are most important in LULC information extraction for a long time (Dean and Smith, 2003; Karnieli et al., 2008). However, these are pixel-based techniques and do not incorporate existing spatial connections among pixels belonging to the same category. Spatial features exhibit the relationship between nearby pixels; that is, the spatial relationships between a central pixel and its nearby counterparts (Dutra and Mascarenhas, 1984).

Texture analysis is one of the commonly used manner using spatial features of an image. In general, the texture is a visual effect, which is created by the spatial distribution of tonal variations in an image (Baraldi and Parmiggirani, 1995). There are apparent textural features in an image and it supplies valuable information for its interpretation (Segl and Kaufmann, 2001; Lillesand et al., 2008). Different textural features are potential source of ancillary information and valuable in improving LULC mapping accuracy (Berberoglu et al., 2000; Rajesh et al., 2001; Herold et al., 2004; Zakeri et al., 2017). A foremost benefit of

using textures in improving classification and mapping accuracy, where new supplementary data sources may not exist, is that textural information can be extracted from the image itself. Many methods have been proposed for the extraction of textural features (Rajesh et al., 2001; Rodriguez-Galiano et al., 2012; Seetharaman and Palanivel, 2013). The gray-level co-occurrence matrix (GLCM) is a widely used manner to extract textural information from images (Haralick et al. 1973). It can be incorporated as supplementary information the same as data bands during the classification procedure (Gong et al. 1992). Textures have been used for various other applications such as crop discrimination (Anys and He, 1995; Soares et al., 1997), estimation of forest biomass and stand age (Kuplich et al., 2005; Cutler et al., 2012; Champion et al., 2014) and identification of plant species (Wang et al., 2004: Wang and Zhang, 2014). The textural features have been investigated extensively and reported in previous research. But, how the selection of textural features is affected by different sensor data with varying spatial resolutions and how it influences LULC classification and accuracy are poorly understood. The identification of suitable textural features for a particular study is a complex task because it requires captivating texture measures, moving window sizes, quantization levels; image bands itself and other aspects into consideration (Chen et al., 2004). But so far, there are no clear guidelines on the selection of an optimal texture due to distinct spatial patterns and compositions of LULC categories in practical projects.

Therefore, textural features have been considered as an effectual source of information to improve classification performance if the optimal textural information can be achieved for a specific investigation. The primary goal of this work is to establish a robust classification process based on texture analysis in accurate mapping of all the major LULC classes considered in a heterogeneous landscape. Specifically, the present work provides a

comprehensive evaluation of textural features from the multi-source data to investigate how the varying spatial resolutions of different sensor data affect the selection of textural elements. Limited studies have been carried out to understand the performance of textural features in improving heterogeneous landscape mapping accuracy and how to efficiently choose suitable textures from multi-sensor and multi-resolution remote sensing data.

3.2 STUDY AREA

This study area is selected because of its highly heterogeneous landscape. The chosen study area provides diverse LULC categories and spatial patterns, which makes it an ideal site to investigate the ideas depicted in this work. The area under study extending from 82° 54′ 30″ to 83° 02′ 30″ E, and from 25° 13′ 08″ to 25° 20′ 43″ N, covering a total area of 253.27 Km^2. The geographical location of study area is shown in Figure 3.1.

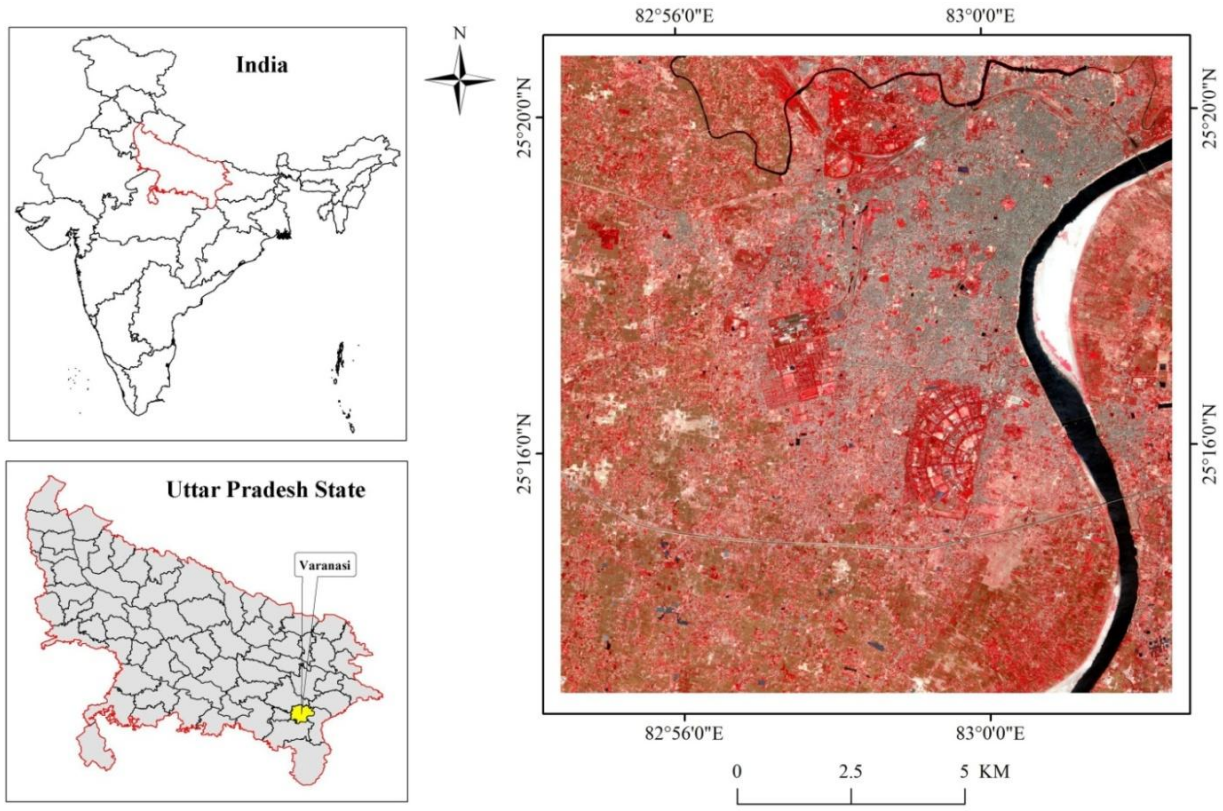

Figure 3.1 Location map of the study area as viewed on LISS-IV FCC image

3.3 METHODOLOGY

3.3.1 Remote sensing data collection and preprocessing

In this work, LISS-IV, Sentinel-1A, LISS-III, RISAT-1 and Landsat 8-OLI images acquired on 06 April 2013, 29 April 2015, 13 March 2013, 01 April 2015 and 15 April 2013 with original pixel sizes of 5.8, 20, 23.5, 25 and 30 m, respectively, were used for comparative analysis of LULC classification of a heterogeneous landscape. The major characteristics of the selected data sets are summarized in Table 1.1.

LISS-IV image has three multispectral bands including two visible (green and red) and one NIR band with 5.8 m spatial resolution. LISS-III image has four bands covering two visible (green and red), one NIR and one SWIR band with 23.5 m spatial resolution. The Landsat 8-OLI imagery has nine spectral bands covering the visible, NIR and SWIR bands with 30 m spatial resolution and one panchromatic band with 15 m spatial resolution. The C-band dual-polarization SAR images, Sentinel-1A (VV, VH) with 20 m and RISAT-1 (HH, HV) with 25 m spatial resolutions are used in this study.

The pre-processing of RISAT-1 image was carried out by using ENVI-SARscape (version 5.1) software. It was multi-looked 2 times in azimuth and 1 times in range direction. Speckles were reduced using the Lee filtering algorithm with 5 × 5 window size. After that RISAT-1 DN image was converted into the backscattering coefficient (σ°) image using Equation (2.1).

The Sentinels Application Platform (SNAP) software (version 3.0.0) freely downloaded (http://step.esa.int/main/download/) was used for the pre-processing of Sentinel-1A image. The image was radiometrically calibrated, and refined lee filter was applied for the speckle

reduction. After speckle reduction, geometric correction was performed and the DN values were converted into backscattering coefficient (σ°).

For the study area, LISS-IV image was chosen as the reference and the other images were georectified to that image using image-to-image registration process. A second order polynomial equation was applied, and images were resampled using nearest neighbor resampling technique. All the images were spatially referenced in the UTM projection system (Zone 44, North) with datum WGS 84. For the LISS-IV image, high data redundancy was found between visible bands B2 and B3 (the correlation coefficient is 0.98). The intra band correlation coefficients in LISS-III and Landsat 8-OLI images were also found to be very similar. For both the images, B2 is highly correlated with all other bands (Venkateswarlu et al., 2014). Because of the large volume data sets and time required for image processing, B2 of LISS-IV, LISS-III and Landsat 8-OLI images was not used during the extraction of textural features in this study.

3.3.2 Field data collection and map legend definition

In addition to remote sensing images, an extensive field survey was undertaken across the study area to collect LULC ground data using handheld GPS receiver. Additionally, to assist in the processes of geometric rectification, the GPS points were collected at road crossings and other man-made features on the ground. In order to accomplish an accurate classification based on remote sensing images, it is significant to define broad LULC classes that are considered to be most suitable for representation of the landscape of study area. Finally, seven broad LULC classes: agricultural land, dense vegetation, sparse vegetation, built-up, fallow land, water bodies and sand are depicted based on prior field knowledge and visual examination of the study area. During field survey, ground truth data were collected

and employed to generate the respective region of interest (ROI) polygons using ENVI 5.1 image analysis software. A part of the data set was used as training data for LULC classification whereas; the remaining data were used as testing data for the assessment of classification results. A well distributed training data were selected randomly for various LULC classes representing the entire study area. In total, 2190 pixels were used as the training data, whereas 730 pixels were employed as the testing data for SVM classification algorithm. The number of training and testing data-sets is given in Table 3.1.

Table 3.1 Number of training and testing pixels for the SVM algorithm

	Agricultural land	Dense vegetation	Sparse vegetation	Fallow land	Built up	Water bodies	Sand	Total
Number of training pixels	303	306	321	312	315	318	315	2190
Number of testing pixels	101	102	107	104	105	106	105	730

3.3.3 Extraction of textural features

Texture analysis has been used broadly to characterize various land surface features from remote sensing images (Solberg and Jain, 1997). The GLCM proposed by (Haralick et al., 1973) is a most commonly used method and employed to extract textural features from remote sensing images. Therefore, eight GLCM-based textural features (i.e., mean, variance, contrast, entropy, homogeneity, dissimilarity, angular second moment and correlation) with seven different window sizes (3x3, 5x5, 7x7, 9x9, 11x11, 13x13 and 15x15), were extracted and tested in this study. Their relevant formulae are listed in Table 1.3. But it is a difficult task to identify suitable textural features for a specific study region, because a good texture is

a inclusive combination of different aspects like texture measure, window size, image band, quantization level, inter-pixel distance (Shaban and Dikshit, 2001; Lu and Weng, 2007). It is closely related to the characteristics of the landscape under investigation as well.

3.3.4 Selection of suitable textural features

A single textural feature is inadequate to mine the spatial features efficiently; however, a combination of two textural features can supply ample ability. Adding more textural features does not considerably improve the LULC mapping accuracy (Shaban and Dikshit 2001; Lu et al., 2008). The inter class separability analysis based on training data, using the transformed divergence method was employed to recognize the potential combinations of two textural features. It was established that using two textural features adequately improved the separability between two LULC categories (Lu et al., 2014). Since all the combinations of textural features were not needed, it was obligatory to develop an appropriate method for the selection of combination of textural features to have the richest source of information for LULC classification. A method to select best combination of textural features, based on standard deviation and correlation coefficients is given by Equation (2.4).

3.3.5 SVM based LULC classification

SVM is a non-parametric supervised classification technique that does not make any assumption regarding the underlying data distribution. SVM has spearheaded its use in various applications due to its robustness, unlike other non-parametric classifiers. Basically, SVM is based on the generation of a separating hyperplane that shows the optimal separation of linearly-separable classes in decision boundary space (Pal and Mather, 2005). But the land surface features classes projected to the input space are not always linearly separable. SVM is able to manage such datasets by the nonlinear projection of the training data in the input

space into a higher dimensional feature space using kernel functions. From Szuster et al., (2011), suppose a set of training data with k number of samples is represented as:

$$\{x_i, y_i\}, i = 1 \ldots . k \tag{3.1}$$

where $x \in R^n$ is an n-dimensional vector and $y \in \{-1, +1\}$ showing the label of each class. This training data set can be separated linearly by a hyperplane if a vector *w* and a scalar *b* can satisfy two inequalities given as follows:

$$w \times x_i + b \geq +1 \quad \text{for all } y = +1 \tag{3.2}$$

$$w \times x_i + b \leq -1 \quad \text{for all } y = -1 \tag{3.3}$$

These two equations can be combined to represent a constraint that must be satisfied to get a hyperplane that completely and linearly separates the two classes in the following equation:

$$y_i(w \times x_i + b) - 1 \geq 0 \tag{3.4}$$

If the two classes are not linearly separable, a set of slack variables $\{\xi_i\}_i = 1$ is introduced to minimize the classification errors where the pixels are classified onto the wrong class hyperplane and is given as:

$$y_i(w \times x_i + b) \geq 1 - \xi_i, \xi_i \geq 0 \tag{3.5}$$

Because this constraint can be met by repetitively increasing the value of ξ_i, a function $C\sum_{i=1} \xi_i$, is added to penalize the solutions which show a large value for ξ_i.

Here, the constant *C* is utilized to control the degree of the penalty managed for the pixels that occur on the wrong side of the separating hyperplane and, as such, the optimization problem becomes:

$$\text{Min}\left[\left(\|w\|^2/_2\right) + C\sum_{i=1} \xi_i\right] \tag{3.6}$$

A mapping function Φ is used to map nonlinear data into a higher-dimensional feature space for the generation of a linearly separating hyperplane. Therefore, input data is represented as $\Phi(x)$, which is the conversion of input vector *x* in feature space into a constructed space with *n* dimensions. It can be computationally costly as *n* increases, so a kernel function is preferred:

$$K(x_i, x_j) = \Phi(x_i) \times \Phi(x_j) \quad (3.7)$$

This kernel function permits the training data to be projected in a larger feature space where it may be increasingly likely to determine a superior margin for the separating hyperplane. There are four commonly used SVM kernels namely: *linear, polynomial, radial basis function (RBF) and sigmoid*. The selection of kernel function and parameters used for a problem and is based on its effect on the speed and accuracy of the classification. The RBF kernel was applied in this study due to its less computational work and ability to handle the non-linear relationship between the training data and the entire dataset. The RBF kernel is given as:

$$\text{Radial basis function}: K(x_i, x_j) = \exp\left(-\gamma \left\| (x_i, x_j) \right\|^2\right), \gamma > 0 \quad (3.8)$$

where γ is the gamma term in the kernel function.

For RBF kernel the penalty parameter (C) was set to its maximum value (i.e. 1000), and gamma parameter (γ) is equal to the inverse of the number of bands (spectral+ textural) of each image. The value of pyramid parameter was set to be zero to process the image at full resolution. The penalty parameter manages the trade-off between margin and misclassification error, while the gamma parameter handles the width of the kernel function (Cortes and Vapnik, 1995). In this study, SVM classification strategy was applied using

ENVI (v 5.1) image processing software. The working scheme for the present work is shown in Figure 3.2.

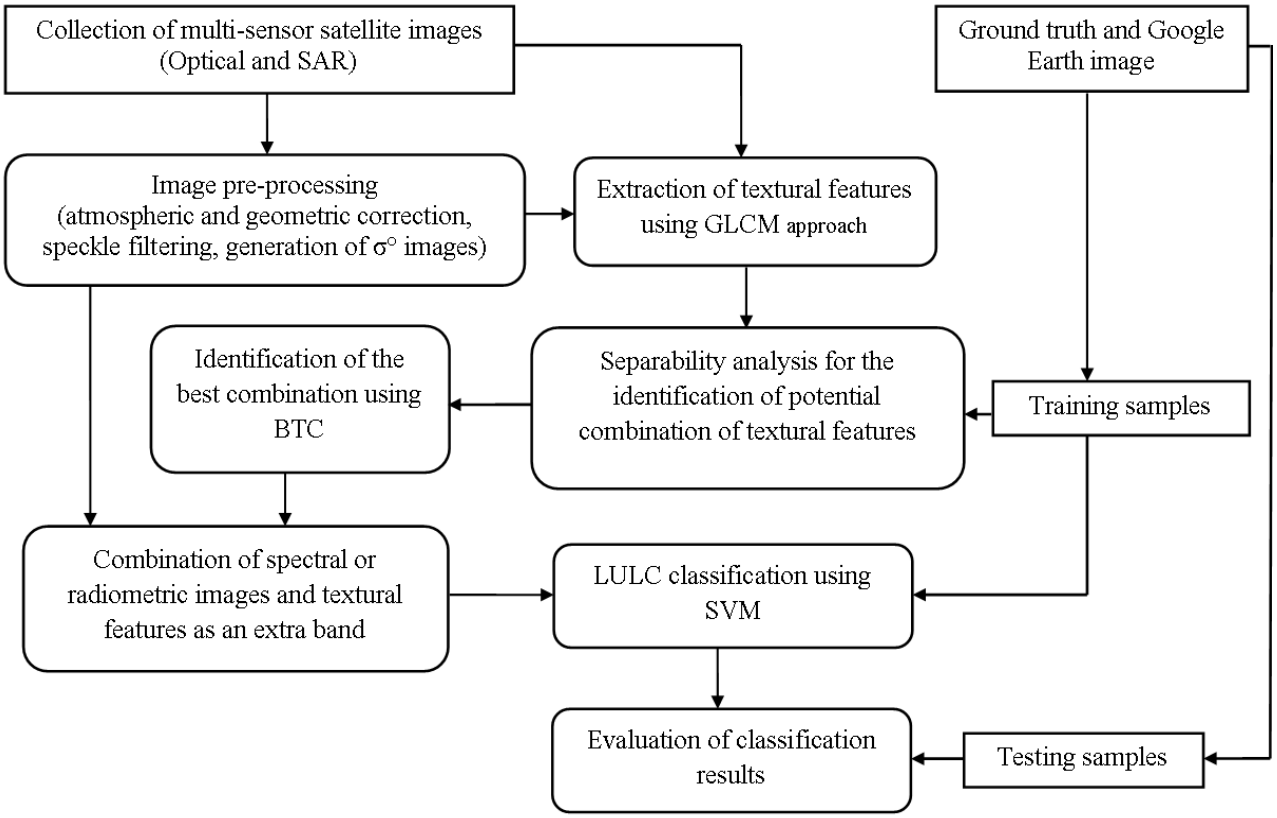

Figure 3.2 Overview of the methodology adopted for this study

3.3.6 Evaluation of LULC classification results

The statistics based on confusion matrix are commonly applied to evaluate the LULC classification results. Consequently, UA, PA, OA, and Kc are then computed using Equations (1.1) to (1.4). The UA and PA are commonly used to evaluate the class-level accuracy, but sometimes this may lead to error because, for some LULC classes, the PA may be high, but the UA may be low, or vice versa. In this study, accuracy measures such as MAH, MAS, ICSI and CSI suggested by Liu et al. (2007) were adopted for more comprehensive evaluation of classification results using Equations (1.6) to (1.9) respectively.

3.4. RESULTS AND DISCUSSION

The work presented here aims to classify and map various land surface elements based on textural features in a heterogeneous landscape. The multi-sensor and multi-resolution data sets were utilized to appraise the performance of the textural features in improving landscape classification and mapping accuracy using SVM classifier. The comparison and appraisal of the outcomes from the optical and SAR sensors are presented as follows.

3.4.1 Analysis of the best combination of textural features

The best combination of textural features for every sensor data was attained based on BTC for potential textural measures. The consequences are reviewed in Table 3.2. The combination of best textural features varies for different sensor data. The Table provides some central insights of the selection of textural features and window sizes. A window sizes of 13x13 and 11x11 were found to be appropriate for the data from optical and SAR sensors respectively. The Mean, dissimilarity, and entropy texture features appeared good for optical sensor data, while mean, variance, contrast and dissimilarity seems suitable for SAR sensor data. Table 3.2 shows that the combinations of best textural features vary, depending on the particular sensor data. It implies the necessity to recognize the best textural combination corresponding to a specific data set. It is essential to identify specific textural features because of different characteristics of the data from the various sensor and different environmental condition of study areas. Therefore, it is a challenging assignment to identify best textural features quickly for a specific study.

Table 3.2 Selected best combination of textural features for LULC classification

Satellite/sensor	Bands/ Polarization	Textural features	Window size (s)	Best textural feature combination
Landsat 8-OLI	NIR	MEA, DIS	9x9	NIR-MEA9, NIR-DIS9
Resourcesat 2-LISS-III	NIR, SWIR	MEA, DIS	9x9	NIR-MEA9, SWIR-DIS9
RISAT-1	HH	MEA, CON	3x3, 7x7	HH-MEA7, HH-CON3
	HV	CON, MEA	3x3, 7x7	HV-MEA7, HV-CON3
Sentinel-1A	VV	VAR, CON	3x3, 11x11	VV-VAR11, VV-CON3
	VH	VAR, CON	3x3, 11x11	VH-VAR11, VH-CON3
Resourcesat 2-LISS-IV	Red, NIR	MEA, ENT	13x13	Red-ENT13, NIR-MEA13

Figure 3.3 represents a comparison of textural images using different texture measure with various bands but same window size (13x13), implying the significance of using best window size in extracting different land surface features. The textural image based on the red band (i.e., LISS-IV band 3) shown in Figure 3.3 (c) highlights the difference between vegetated and non-vegetated land surface features. The textural image based on the NIR band (i.e., LISS-IV band 4) shown in Figure 3.3 (d) highlights the built up, sparse vegetation and fallow land classes. Figure 3.4 illustrates the textural images that are calculated using different measures with different bands but the same window size (9 × 9), implying different abilities in the extraction of land surface features. Figure 3.5 provides a comparison of textural images using different texture measure but same window size (9x9), implying the significance of using best window size in extracting different land surface features. The textural image based on the NIR band (i.e., Landsat 8-OLI band 5) shown in Figure 3.5 (b) highlights the non-vegetated surfaces like built up area, water bodies, and roads. Figure 3.6 compares the RISAT-1 HH and HV, and their corresponding two textural features, representing their complementary information. It can be seen that, the textural features from

RISAT-1 contain much less information in comparison to optical images, indicating that the RISAT-1-based textural features have less ability for representing the characteristics of land surface features. Figure 3.7 compares Sentinel-1A VV and VH, and their corresponding two textural features, representing their complementary information. It can be seen that the textural features from Sentinel-1A contain much less information in comparison to optical images, indicating its less ability for representing the characteristics of land surface features.

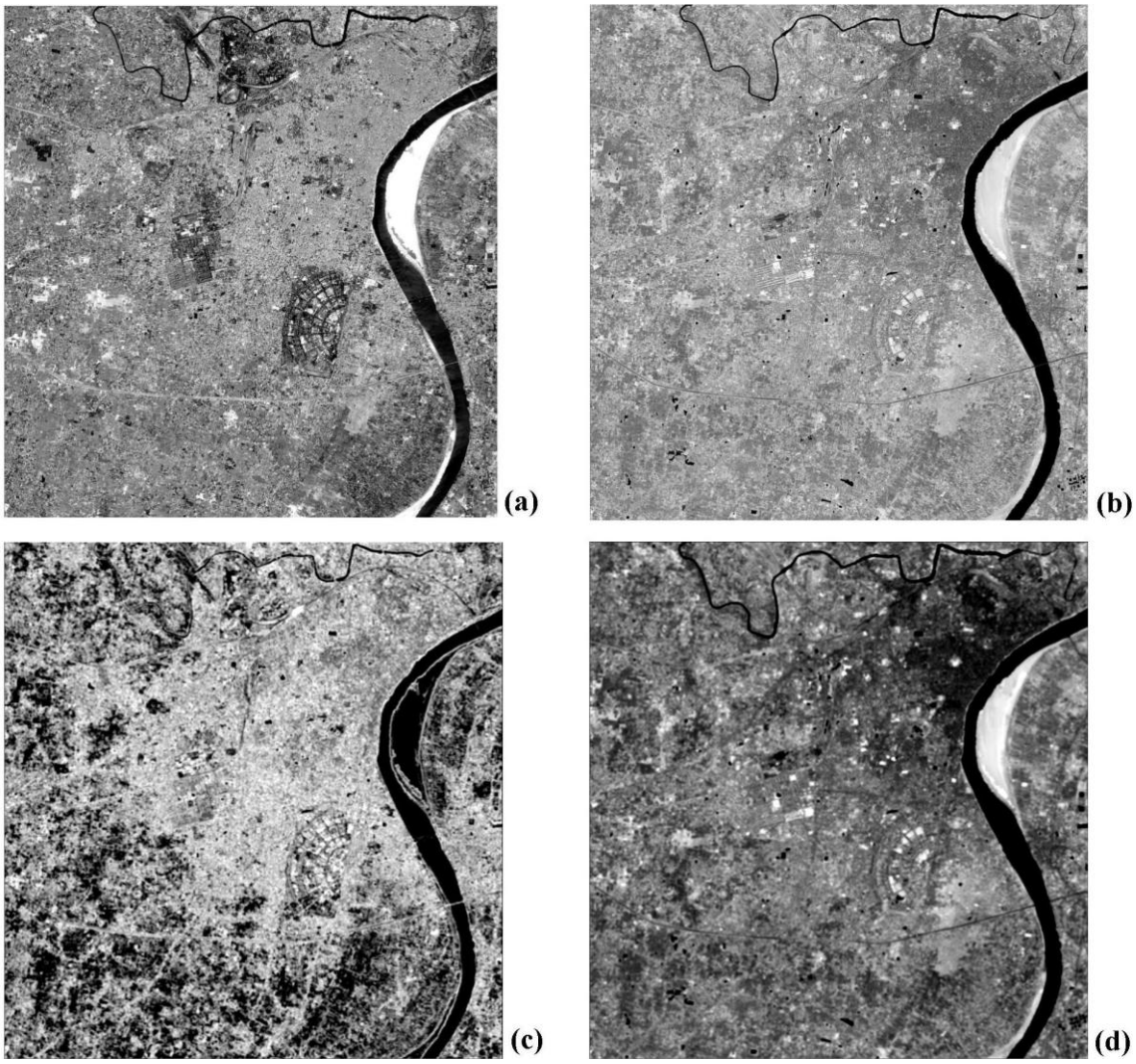

Figure 3.3 Comparison of (a) LISS-IV B3 (Red), (b) LISS-IV band 4 (NIR), (c) textural image obtained using the measure 'entropy' on B3 (Red) and a window size of 13 × 13 pixels, and (c) textural image obtained using 'mean' on B4 (NIR) and window size of 13× 13 pixels.

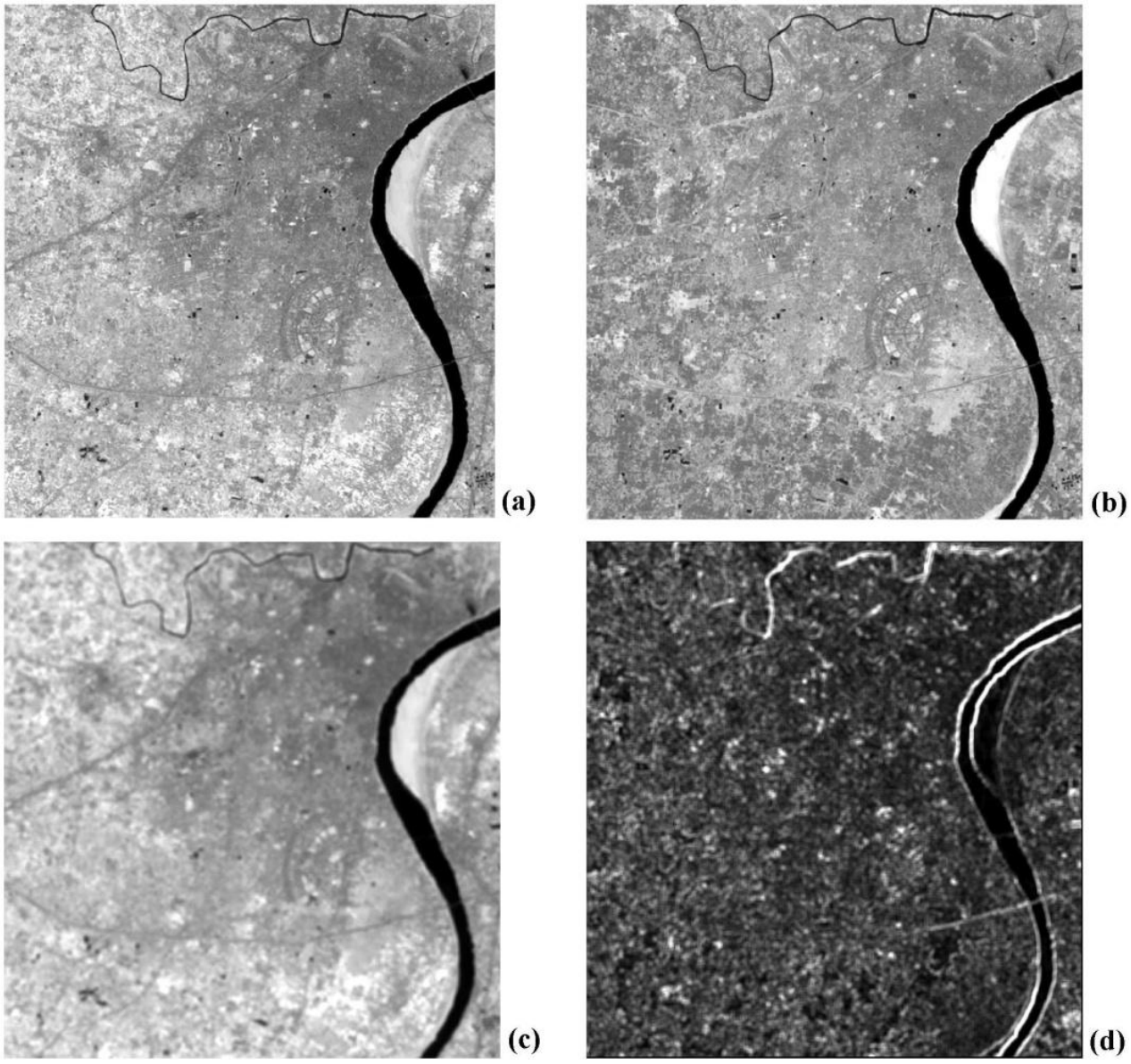

Figure 3.4 Comparison of (a) LISS-III B4 (NIR), (b) LISS-III B5 (SWIR), (c) textural image obtained using the measure 'mean' on B4 (NIR) and a window size of 9 × 9 pixels, and (c) textural image obtained using 'dissimilarity' on B5 (SWIR) and window size of 9× 9 pixels.

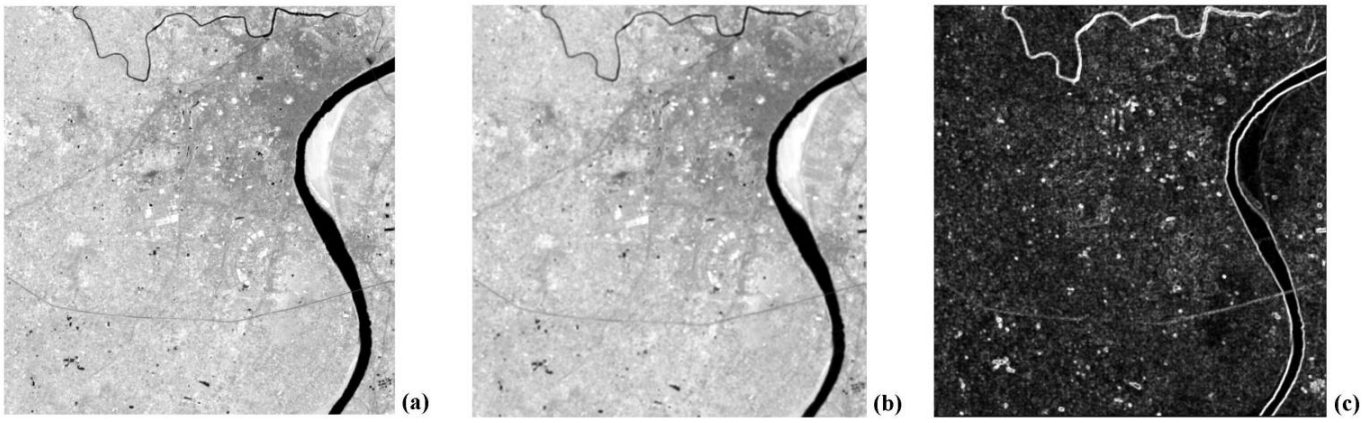

Figure 3.5 Comparison of (a) Landsat 8-OLI B5 (NIR), (b) textural image obtained using the measure 'mean' on B5 (NIR) and a window size of 9 × 9 pixels, and (c) textural image obtained using 'dissimilarity' on B5 (NIR) and window size of 9× 9 pixels.

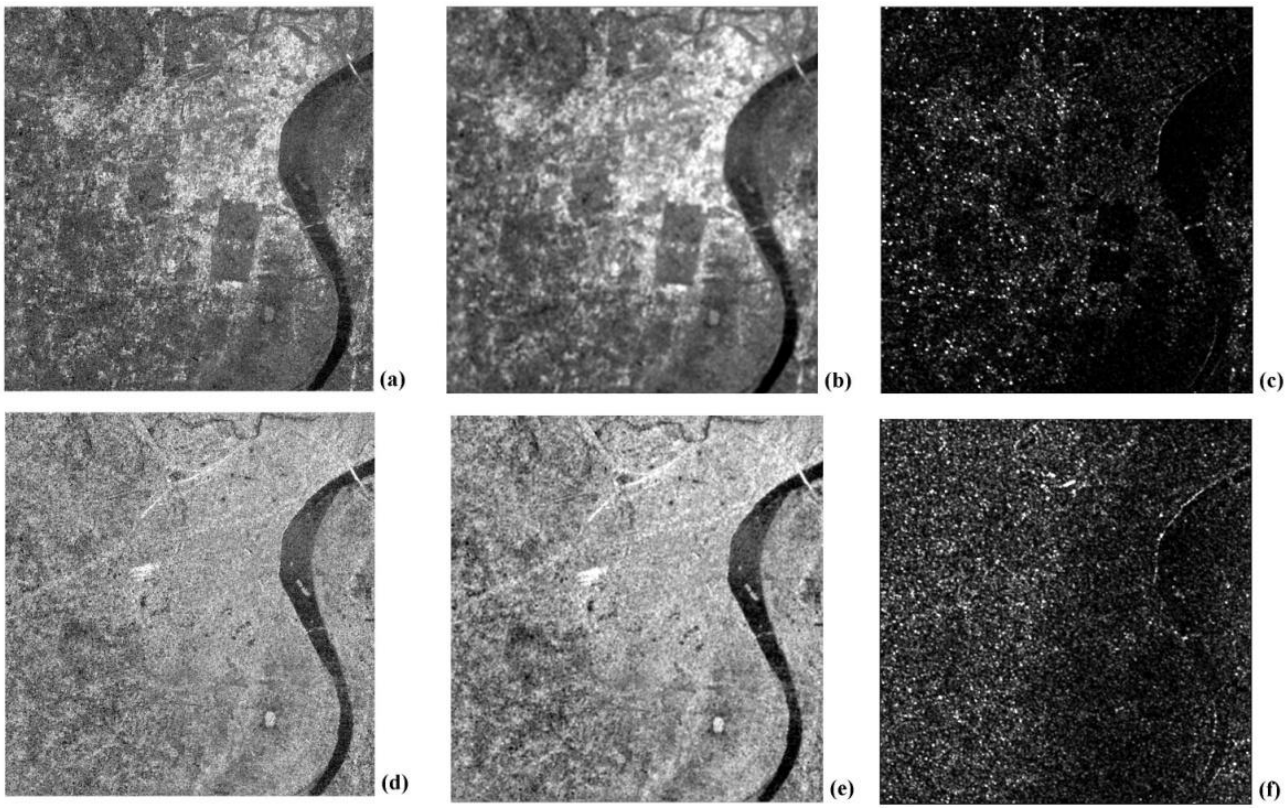

Figure 3.6 Comparison between RISAT-1 C-band HH and HV images and corresponding textural images; (a), (b), and (c) are HH image and HH-derived MEA7 and CON3 textural images; (d), (e), and (f) are HV image and HV-derived MEA7 and CON3 textural images.

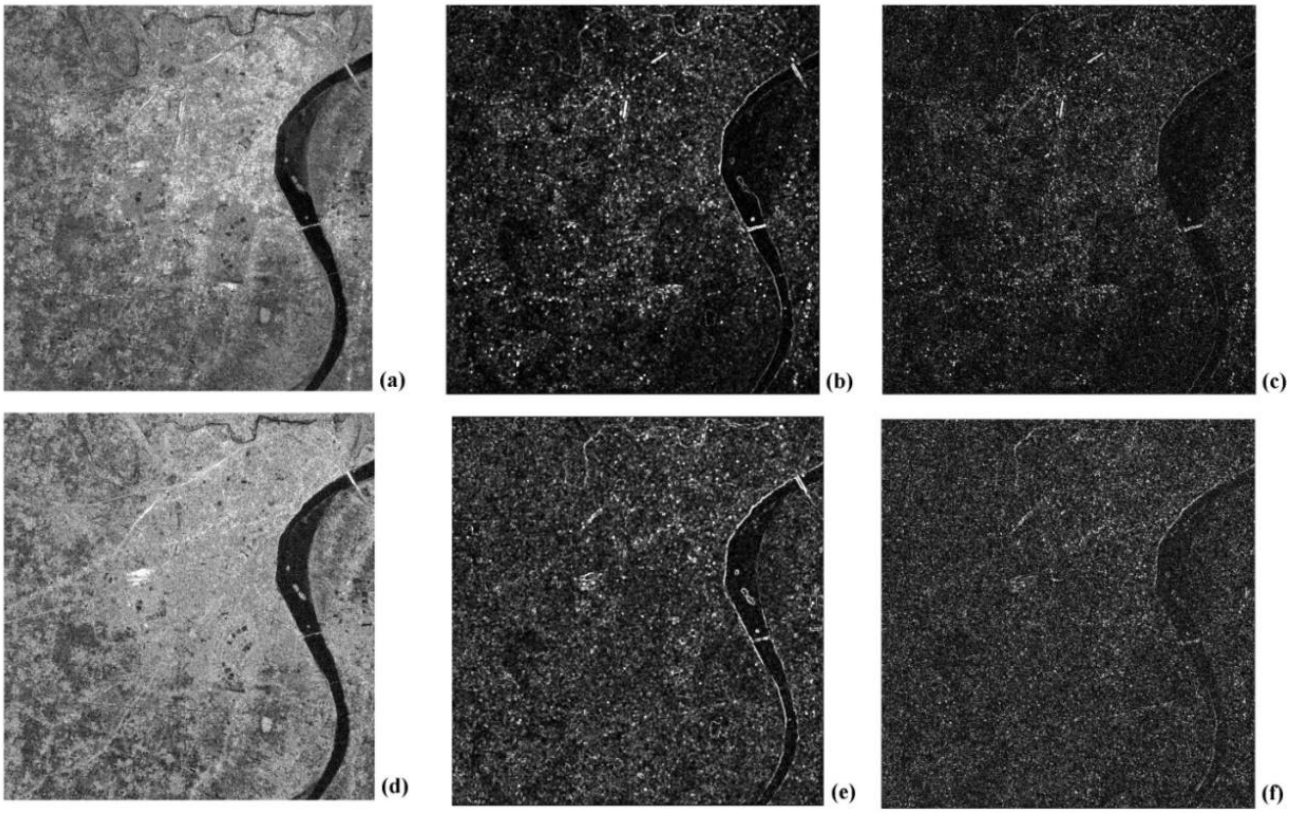

Figure 3.7 Comparison between Sentinel-1A C-band VV and VH images and corresponding textural images; (a), (b), and (c) are VV image and VV-derived VAR11 and CON3 textural images; (d), (e), and (f) are VH image and VH-derived VAR11 and CON3 textural images.

3.4.2 Analysis of overall LULC classification results using textural features

The multispectral optical images provided enhanced classification accuracy than SAR images. For high spatial resolution LISS-IV image, only with spectral information can lead to unsatisfactory results. It is due to the spectral confusion within the vegetation categories specifically agricultural land and sparse vegetation. This problem can be reduced by using textural features in combination with spectral information of vegetation categories. Table 3.3 shows the LULC classification results for LISS-IV image in terms of UA, PA, MAH, MAS, and ICSI. The OA based on spectral images was 88.49% with Kc 0.866 and CSI 76.97%.

However, the incorporation of textural features into spectral images improved the OA and CSI by 6.72% and 13.44% respectively. It is also evident that the combination of spectral and textural features improved the UA of agricultural land and sparse vegetation from 85.58% to 93.27% and from 83.02% to 95.19% respectively. For other LULC classes, the classification accuracy is improved significantly by incorporating textural features into multispectral data, implying the significance of textural images for images with high spatial resolution.

The multispectral LISS-III and Landsat 8-OLI images based on spectral information provided good OA with 85.34% and 85.62% respectively. Table 3.4 shows the LULC classification results for LISS-III image. However, integration of textural features into spectral image improved OA by 3.84% from 85.34% to 89.18%. When considering individual LULC classes, almost all of the classes, except dense vegetation showed significant improvement in classification results by incorporating textural features. When the overall classification accuracy is evaluated using CSI, the accuracy was improved by 7.64% from 70.70% to 78.34%. Table 3.5 shows the LULC classification results for Landsat 8-OLI image. However, integration of textural features into spectral images improved OA by 4.11% from 85.62% to 89.73%. When considering individual LULC classes, almost all of the classes, except agricultural land and sparse vegetation showed significant improvement in classification accuracy by incorporating textural features. When the overall classification accuracy is evaluated using CSI, it was improved by 8.10% from 71.40% to 79.50%. It is remarkable to note that the textural features are vital in improving classification accuracy, but not for all LULC categories.

The SAR images provided lower OA in comparison to multispectral optical images of the same area. The classification results for the RISAT-1 image are summarized in Table 3.6.

The radiometric data of RISAT-1 can only provide reasonable accuracy for sparse vegetation, built up and water bodies. But the combination of radiometric data with textural features enhanced the OA by 8.22% from 78.49% to 86.71%, and CSI by 16.19% from 57.24% to 73.43%. The classification results for Sentinel-1A image are summarized in Table 3.7. The radiometric data of Sentinel-1A can only provide reasonable accuracy for dense vegetation, fallow land, built up and water bodies. But the combination of radiometric data with textural features improved the OA by 7.43% from 80.27% to 87.27%, and CSI by 14.31% from 61.25% to 75.56%. The classification products achieved by using SVM algorithm are shown in Figure 3.8 (a-e).

Table 3.3 Comparison of accuracy assessment results using LISS-IV image

LULC class	Spectral bands					Spectral bands + textural features				
	PA (%)	UA (%)	MAH (%)	MAS (%)	ICSI (%)	PA (%)	UA (%)	MAH (%)	MAS (%)	ICSI (%)
Agricultural land	88.12	85.58	86.83	76.72	73.70	96.04	93.27	94.63	89.81	89.31
Dense vegetation	93.14	91.35	92.23	85.59	84.48	98.04	95.24	96.62	93.46	93.28
Sparse vegetation	82.24	83.02	82.63	70.40	65.26	92.52	95.19	93.84	88.39	87.72
Fallow land	80.77	84.85	82.76	70.59	65.62	90.38	94.95	92.61	86.24	85.33
Built up	91.43	90.57	91.00	83.48	81.99	97.14	94.44	95.77	91.89	91.59
Water bodies	95.28	91.82	93.52	87.83	87.10	99.06	97.22	98.13	96.33	96.28
Sand	88.57	92.08	90.29	82.30	80.65	93.33	96.08	94.69	89.91	89.41
OA (%)			88.49					95.21		
Kc			0.866					0.944		
CSI (%)			76.97					90.41		

Table 3.4 Comparison of accuracy assessment results using LISS-III image

LULC class	Spectral bands					Spectral bands + textural features				
	PA (%)	UA (%)	MAH (%)	MAS (%)	ICSI (%)	PA (%)	UA (%)	MAH (%)	MAS (%)	ICSI (%)
Agricultural land	78.22	81.44	79.80	66.39	59.66	82.18	88.30	85.13	74.11	70.48
Dense vegetation	88.24	90.91	89.55	81.08	79.14	93.14	93.14	93.14	87.16	86.27
Sparse vegetation	78.90	79.63	79.26	65.65	58.53	83.18	83.96	83.57	71.77	67.14
Fallow land	79.81	78.30	79.05	65.35	58.11	86.54	84.91	85.71	75.00	71.44
Built up	91.43	85.71	88.48	79.34	77.14	95.24	89.29	92.17	85.47	84.52
Water bodies	94.34	93.46	93.90	88.50	87.80	96.23	92.73	94.44	89.77	88.95
Sand	86.41	88.12	87.25	77.39	74.53	87.62	92.00	89.76	81.42	79.62
OA (%)			85.34					89.18		
Kc			0.829					0.874		
CSI (%)			70.70					78.35		

Table 3.5 Comparison of accuracy assessment results using Landsat 8-OLI image

LULC class	Spectral bands					Spectral bands + textural features				
	PA (%)	UA (%)	MAH (%)	MAS (%)	ICSI (%)	PA (%)	UA (%)	MAH (%)	MAS (%)	ICSI (%)
Agricultural land	84.16	91.40	87.63	77.98	75.56	90.10	92.86	91.46	84.26	82.96
Dense vegetation	88.24	90.91	89.55	81.08	79.14	93.14	94.06	93.60	87.96	87.20
Sparse vegetation	85.98	82.88	84.40	73.02	68.86	90.65	84.35	87.39	77.60	75.00
Fallow land	76.92	76.92	76.92	62.50	53.85	77.88	84.38	81.00	68.07	62.26
Built up	88.57	86.11	87.32	77.50	74.68	93.33	90.74	92.02	85.22	84.07
Water bodies	89.62	91.35	90.48	82.61	80.97	94.34	95.24	94.79	90.09	89.58
Sand	85.71	81.08	83.33	71.43	66.80	88.57	86.92	87.74	78.15	75.49
OA (%)			85.62					89.73		
Kc			0.832					0.880		
CSI (%)			71.41					79.51		

Table 3.6 Comparison of accuracy assessment results using RISAT-1 image

LULC class	Radiometric bands					Radiometric bands + textural features				
	PA (%)	UA (%)	MAH (%)	MAS (%)	ICSI (%)	PA (%)	UA (%)	MAH (%)	MAS (%)	ICSI (%)
Agricultural land	77.23	74.29	75.73	60.94	51.51	84.16	83.33	83.75	72.03	67.49
Dense vegetation	80.39	78.85	79.61	66.13	59.24	90.20	85.98	88.04	78.63	76.18
Sparse vegetation	67.29	81.82	73.85	58.54	49.11	75.70	87.10	81.00	68.07	62.80
Fallow land	72.12	73.53	72.82	57.25	45.64	80.77	81.55	81.16	68.29	62.32
Built up	88.57	86.92	87.74	78.15	75.49	97.14	96.23	96.68	93.58	93.37
Water bodies	80.19	84.16	82.13	69.67	64.35	90.57	89.72	90.14	82.05	80.29
Sand	83.81	71.19	77.19	62.86	55.35	88.57	83.04	85.71	75.00	71.61
OA (%)			78.49					86.71		
Kc			0.749					0.845		
CSI (%)			57.24					73.44		

Table 3.7 Comparison of accuracy assessment results using Sentinel-1A image

LULC class	Radiometric bands					Radiometric bands + textural features				
	PA (%)	UA (%)	MAH (%)	MAS (%)	ICSI (%)	PA (%)	UA (%)	MAH (%)	MAS (%)	ICSI (%)
Agricultural land	72.32	77.88	75.00	60.00	50.21	82.57	86.54	84.51	73.17	69.11
Dense vegetation	87.64	80.41	83.87	72.22	68.05	91.58	86.14	88.78	79.82	77.72
Sparse vegetation	71.90	77.68	74.68	59.59	49.58	83.33	86.36	84.82	73.64	69.70
Fallow land	72.73	80.90	76.60	62.07	53.63	79.61	90.11	84.54	73.21	69.72
Built up	94.68	89.90	92.23	85.58	84.58	96.00	92.31	94.12	88.89	88.31
Water bodies	90.18	84.17	87.07	77.10	74.35	94.64	89.83	92.17	85.48	84.47
Sand	76.11	74.14	74.14	58.90	48.38	86.92	83.04	84.93	73.81	69.95
OA (%)			80.27					87.70		
Kc			0.770					0.856		
CSI (%)			61.25					75.57		

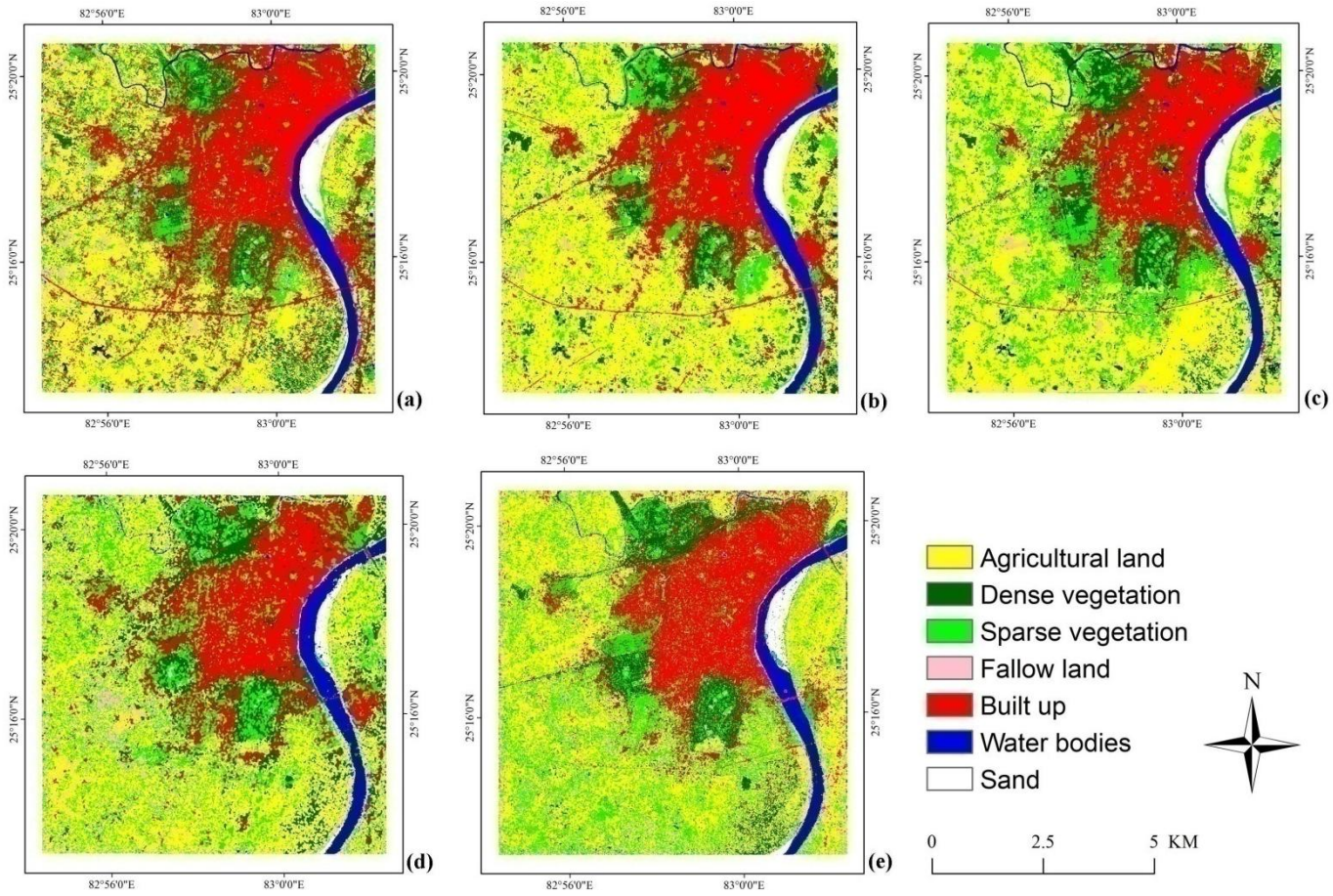

Figure 3.8 Classified LULC maps based on SVM algorithm (a) LISS-IV, (b) LISS-III, (c) Landsat 8-OLI, (d) RISAT-1, and (e) Sentinel-1A

3.4.3 Comparative analysis of overall LULC classification performance among multi-sensor and multi-resolution data

When the results of SAR and optical datasets were compared, textural images obtained from the radiometric data seem to play a more significant role in improving LULC classification accuracy than those from spectral data. A summary of the assessment of overall classification results is provided in Table 3.8. It represents that there are considerably different roles of textural features obtained from different sensor data in improving LULC

classification accuracy. Comparing multispectral optical Landsat 8-OLI data at 30 m to LISS-IV data at 5.8 m, the CSI increased from 8.10% to 13.44%, suggesting the significantly important role of textural features in improving LULC classification accuracy with increased spatial resolution of the optical sensor data. Incorporation of textural features into SAR sensor data is particularly valuable in improving classification accuracy compared to optical sensor data. For RISAT-1 and LISS-III data with almost same spatial resolution, the CSI of the RISAT-1 data was improved by 16.19% compared to the 7.64% improvement in that of the LISS-III data. It implies the crucial role of texture features in reducing speckles and also the inherent heterogeneity within the same LULC category in RISAT-1 data.

Table 3.8 Summary of overall classification accuracies for multi-sensor data

		CSI (%)		
Sensor name	Pixel size (m)	Original bands	Combination	Improvement in CSI (%)
Landsat 8-OLI	30	71.41	79.50	8.09
RISAT-1	25	57.24	73.44	16.20
LISS-III	23.5	70.70	78.35	7.65
Sentinel-1A	20	61.25	75.57	14.32
LISS-IV	5.8	76.97	90.41	13.44

Although, we recognized that the textural features are much crucial in improving LULC classification and mapping accuracy. But for a specific study, the difficulties and challenges appeared during the identification of suitable textural features due to its dependency on particular sensor data used and the attributes of the landscapes under examination. Therefore, the automatic selection of textural features in a particular study is still a complicated task due to the lack of general guidelines. Since the performance of textural features depends on the complex combination of texture measures, the specific sensor data, window size, and the LULC categories present. It is beneficial to incorporate textural features into spectral or

radiometric images in improving classification accuracy, but not for all LULC categories. Use of textural information may improve the classification accuracy of some LULC categories such as agricultural land and sparse vegetation by reducing their spectrally similar response. The findings of present work are promising because the accurate mapping of heterogeneous landscapes is a very challenging task. Further research is required to perform a comparative analysis between images having different spatial resolutions for other landscape and classification methods.

3.5 CONCLUSION

The present research explores the efficacy of incorporating textural features into spectral or radiometric images in enhancing the LULC classification accuracy of heterogeneous landscape using multi-sensor and multi-resolution data. The ability of textural features in reducing speckles and inherent heterogeneity within the same landscape category makes it significant for LULC classification using SAR data and high spatial resolution multispectral LISS-IV data. It is essential to recognize the textural features that have good separability for LULC categories but low correlation between them. Textural features have less capability for discriminating LULC categories than spectral images, particularly for medium spatial resolution images. But the textural features become more valuable with increasing spatial resolution. The CSI can be improved from 8.10% to 13.44% as the spatial resolution decreases from 30 m to 5.8 m. It is also observed that the incorporation of textural features into SAR sensor data is particularly valuable in improving the classification accuracy compared to optical sensor data. Furthermore, it is needed to develop new methods to perform an automatic selection of optimal combinations of textural features for a specific study purpose.